Deep potential for interaction between hydrated Cs$^+$ and graphene

Yangjun Qin[1,2], Xiao Wan[1], Liuhua Mu[3,4], Zhicheng Zong[1,2], Tianhao Li[1,2], Nuo Yang[2, †]

1) School of Energy and Power Engineering, Huazhong University of Science and Technology, Wuhan 430074, China

2) Department of Physics, National University of Defense Technology, Changsha 410073, China

3) Wenzhou Institute, University of Chinese Academy of Sciences, Wenzhou 325001, China.

4) School of Physical Science, University of Chinese Academy of Sciences, Beijing 100049, China

†Corresponding E-mail: N.Y. (nuo@nudt.edu.cn)

ABSTRACT

The influence of hydrated cation-π interaction forces on the adsorption and filtration capabilities of graphene-based membrane materials is significant. However, the lack of interaction potential between hydrated Cs^+ and graphene limits the scope of adsorption studies. Here, it is developed that a deep neural network potential function model to predict the interaction force between hydrated Cs^+ and graphene. The deep potential has DFT-level accuracy, enabling accurate property prediction. This deep potential is employed to investigate the properties of the graphene surface solution, including the density distribution, mean square displacement, and vibrational power spectrum of water. Furthermore, calculations of the molecular orbital electron distributions indicate the presence of electron migration in the molecular orbitals of graphene and hydrated Cs^+, resulting in a strong electrostatic interaction force. The method provides a powerful tool to study the adsorption behavior of hydrated cations on graphene surfaces and offers a new solution for handling radionuclides.

Introduction

Currently, the global marine ecosystem is facing a significant challenge for radioactive pollution that needs to be addressed[1, 2]. The occurrence of accidents at nuclear facilities and the improper disposal of radioactive waste presents a direct threat to marine organisms and human health[3, 4]. The decontamination of marine environments, particularly the extraction of radioactive pollutants, is a critical yet complex endeavor that is vital for the preservation of the ecological balance and the public health security.

The treatment of radioactive elements in seawater has rapidly developed over the years. Amongst the numerous methodologies employed, adsorption[5] and membrane filtration[3, 6] techniques stand out for their efficiency and ease of operation. These processes serve as potent tools in the arsenal against marine nuclear effluents, finding broad application across diverse sectors.

Adsorption and membrane filtration are highly effective methods for removing radioactive materials and are extensively applied in various fields. Molecular sieves[7], zeolites[8], ion-exchange resins[9], and metal-organic frameworks[10] have emerged as pivotal materials in the efficient sequestration of radiocerium and strontium ions, employing either physical adsorption or chemical bonds strategies. Furthermore, Carbon nanomaterials, when surface-modified[11], enhance ion-material interactions, achieving superior adsorption efficacy. However, the associated costs and operational complexities remain significant hurdles. Graphene, with its unparalleled surface area and cost-effectiveness, emerges as a promising candidate for ion adsorption

membranes[12, 13].

Graphene adsorption research has significantly increased in the past two decades. The strong interaction force between cation and graphene has been gradually recognized[14], despite its notable divergence from the prevailing perception. Molecular dynamics[15, 16], a powerful analytical tool, has been instrumental in elucidating hydrated cation-π interactions[17, 18]. Yet, the absence of a precise potential function to describe these interactions has hindered progress. Fang et al.'s pioneering work, combining quantum mechanics and molecular dynamics, led to the successful calibration of the Na^+-π interaction potential[19, 20]. Their model predicted ion accumulation on graphene surfaces, validating the concept of ion sieving[21]. Other approaches include incorporating cation polarization effects into the empirical potential function[22] and modifying the depth of the potential well for C-Na interactions[23]. Nevertheless, these methodologies have not yet attained the desired level of accuracy, and their practical viability remains to be further discussed and validated.

The interaction potential between hydrated cation is severely limited. In previous, a multitude of quantum mechanical methodologies were employed, encompassing multi-parameter fitting and computations of multi-body interactions, among other sophisticated techniques. However, this approach has been beset with challenges, particularly when applied to the training of potential functions for systems comprising four or more distinct elements, such as hydrated Cs^+ systems. The intricacies and computational demands increase exponentially, rendering the traditional quantum mechanical methods less feasible for such complex systems. Recently, machine

learning methods[24, 25] offer a powerful tool with the computational efficiency of molecular dynamics and the precision of density functional theory (DFT)[26]. Deep potential (DP)[27-30] stands out for its scalability and accuracy in handling large atomic systems than others[31-34]. DP has been employed in diverse fields[35-38]. The adsorption mechanism of radioactive ions on graphene surfaces could be elucidated by the study of DP potentials containing hydrated Cs^+-π interactions, with implications for both fundamental and applied nuclear wastewater treatment research.

This study constructed a potential for hydrated Cs^+-π interaction using the machine learning potential function method. Firstly, the accuracy of the potential function was validated. Secondly, the properties of the graphene surface solution, including the vibrational power spectrum of the water, the density, the radial distribution function, and the mean square displacement (MSD) were calculated. Finally, the density of states of the system was calculated to elucidate the nature of the hydration cs^+-π interaction.

Deep potential

In the DP model, meticulous parameter tuning is paramount to ensure the precision and reliability of the resultant potential function. The DP framework assumed that the potential energy E of any given configuration can be decomposed into the summation of individual atomic contributions E_i, each of which is a function of the local environment descriptor D_i of atom i. This descriptor describes the local environment of atom i within the truncation radius. The truncation radius and smoothing radius are set to 0.6 nm and 0.05 nm, respectively, striking a balance between computational

efficiency and the accuracy of the interatomic potential. The dimensions of the embedding network and the fitted network are (25, 50, 100) and (240, 240, 240), respectively. Furthermore, the hyper-parameters start-pref_e, start-pref_f, start-pref_v, limit-pref_e, limit-pref_f, and limit-pref_v, which regulate the weights of energy and force losses in the total loss function, have been set to 0.02, 1000, 0, 1.0, 1.0, and 0, respectively. The initial learning rate is set at 10^{-3} and decays exponentially to 10^{-8} at the conclusion of the training period. The number of training steps is set to 1,500,000. The functions trained with these optimized parameters have been demonstrated to achieve the training accuracy of DFT[38, 39]. thereby substantiating the rationality and effectiveness of the adopted parameterization strategy.

The initial data obtained in Ab initio molecular dynamics (AIMD) is insufficient to encompass the entirety of the structural phase space. The DP generator package[40, 41] is utilized to orchestrate the Large-scale Atomic/Molecular Massively Parallel Simulator software. This enables an exhaustive exploration of the structural phase space and facilitates the procurement of structurally valid data. So, four models were crudely trained utilizing the preliminary dataset. Subsequently, MD simulations were conducted across the temperature range utilizing a DP model. Within these simulations, a comparative analysis was performed, focusing on the fluctuation of energies and atomic forces exerted by structures at distinct time points. Additionally, one DP model was leveraged to compute predictions for the remaining three potential function models, fostering a comprehensive comparison and validation process. The maximum force deviation δ_f^{max} equations for the four models are as follows:

$$\delta_f^{max} = max_i\sqrt{\langle|F_i - \langle F_i\rangle|^2\rangle} \tag{1}$$

When the atomic force δ_f^{max} is smaller than δ_{low}, the configuration is labeled as exact configuration, while when δ_f^{max} is larger than δ_{high}, the configuration is labeled as failed configuration. When $\delta_{low}<\delta_f^{max}<\delta_{high}$, the configuration is labeled as a candidate configuration, which will be added to the initial data set for training in the next step. A total of 15 iterations were performed throughout the simulation, as detailed in Table S1.

AIMD is performed based on Vienna ab initio simulation package with the Perdew–Burke–Ernzerhof generalized gradient approximation and the projector augmented wave pseudopotentials. The base training dataset was extracted from energy, force and virial data obtained from an ensemble of 2,000 initial configurations. These configurations were subjected to a series of 10-step AIMD simulations. The temperature parameters for these simulations ranged from 200 K to 300 K, and the simulation conditions were 0 Pa with timestep of 0.5 fs[42]. As illustrated in Fig. S1, our study definitively demonstrates that an energy cutoff threshold of 520 eV in conjunction with a k-point spacing of 0.3 Å^{-1} is sufficient to achieve convergence of energy values and atomic forces. The k-point grid has been designed with a size of $3 \times 3 \times 1$, ensuring a balanced trade-off between accuracy and computational efficiency.

The DP-gen was employed to train the interaction potential between hydrated Cs^+ and graphene. As previously outlined, the training process encompasses three key components within the potential function. This iterative training process continues until a precision benchmark of 99% is achieved, at which point the training is terminated. The accuracy of the DP potential function is corroborated by a comparison of the results

with the DFT calculations, as depicted in Fig. 1(a) through 1(d). The data set for training

and validation purposes comprises 7,244 structures and 1,000 structures, respectively.

The root mean square error (RMSE) values, which serve as measures of accuracy, are

reported to be 4.25 meV/atom for the training dataset and 2.58 meV/atom for the

validation dataset, as illustrated in Fig. 1(a) and 1(c). Further analysis in Fig. 1(f)

elucidates the potential function curves for hydrated cation structures, revealing the

concordance between the DFT and DP, as well as illustrating that the universal force

field (UFF)[43] differs significantly from the DP . The high degree of accuracy exhibited

by DP renders them eminently suitable for deployment in molecular dynamics

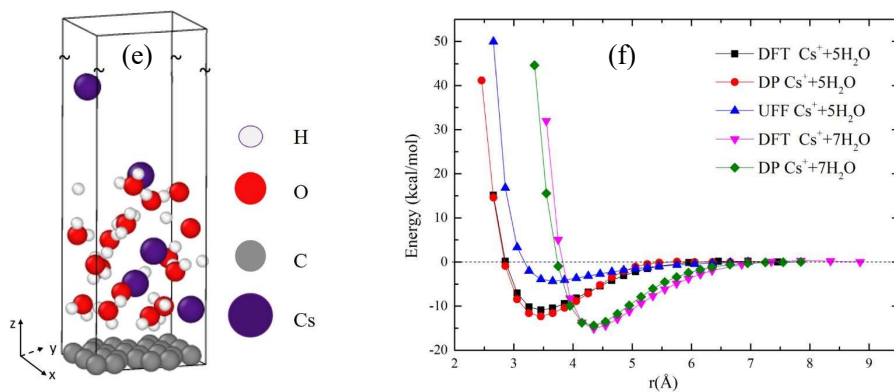simulations, ensuring reliable predictions and insights into complex systems.
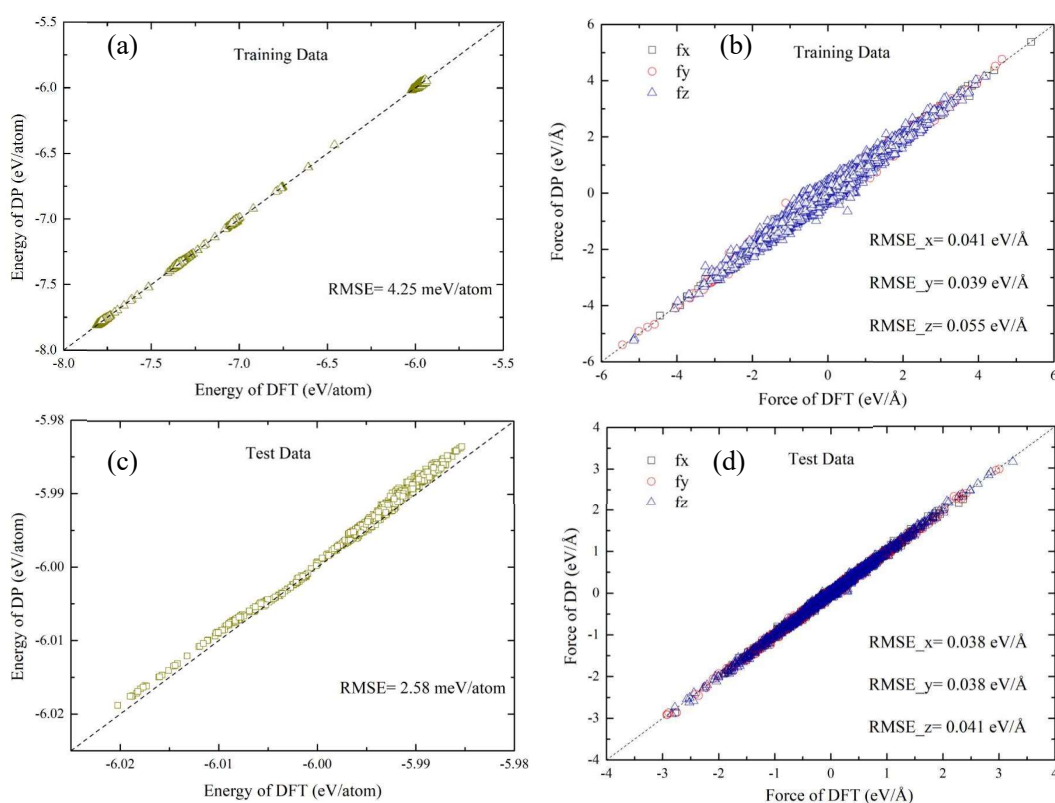
Figure 1. The training and validation results of DP. (a) The system energy by DP (the training set) versus the energy by DFT. (b) The force for the training set in comparison with the results of the DFT calculations. (c) Energy for the test set versus the results of the DFT calculations. (d) Force for the training set versus the results of the DFT calculations. (e) Schematic structure of the system, including H_2O, Cs^+ and graphene. (f) The comparisons of potential function between the hydrated Cs^+ and the graphene, calculated by DFT, DP and UFF.

Simulation results and discussions

The objective of this investigation is to examine the impact of graphene π-bonds on the characteristics of its surface solution and to assess the discrepancies between the DP and UFF for property prediction. Two distinct systems, comprising 3040 atoms, were constructed using molecular dynamics simulations as visualized with OVITO[44] in Fig. 2. A significant distinction between these two systems is that classical molecular dynamics is unable to utilize the UFF for calculations in non-neutral systems, whereas DP does not incorporate the impact of charge in molecular dynamics simulations. Detailed UFF parameters are referenced in Ref.[19],
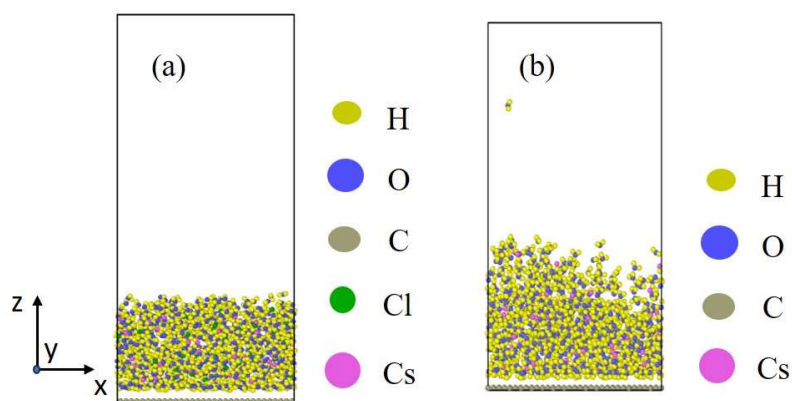

Figure 2. The snapshots of the system. (a) the system of UFF, (b) the system of DP.

The vibrational power spectrum of water is an important parameter of aqueous solutions. Furthermore, this section examines the impact of graphene π-bonds on the vibrational power spectrum of aqueous solutions, which facilitates an understanding of molecular vibrations. The vibrational power spectrum of a water molecule is determined through Fourier transformation of the autocorrelation function of the velocity of water. The latter can be expressed as [45]:

$$I(v) \propto \lim_{\tau \to \infty} \int_{-\tau}^{\tau} \langle v_i(t_0 + t) \cdot v_j(t_0) \rangle e^{-i2\pi vt} dt \tag{2}$$

where I is the intensity, v is the vibrational frequency, and v is the velocity of the atom. After counting the data for another 50 ps and calculating the vibrational power spectrum of water containing two regions: the range of 2 nm to 4 nm (region 1) and the range of 0.6 nm from the graphene wall (region 2).

It is investigated that the effect of π-bonds in graphene on the vibrational power spectrum of water molecules. As illustrated in Fig. 3(a), the velocity spectrum reveals a multiplicity of distinct peaks, each attributable to specific interactions: hydrogen bonding, the H-O-H bend angle, and O-H bond formation, respectively. A comparison of the theoretical and experimental data reveals a clear agreement between the peak frequencies of the water vibration power spectrum in region 1 and the corresponding experimental[46, 47]. In the high-frequency range, the vibrational power spectrum of water in region 2, in proximity to graphene, is observed to be redshifted. The vibrational power spectrum of water molecules, as portrayed in Fig.S3, was computed under the application of UFF. It has been revealed through the investigations that there exists a considerable disparity between these computations and experimental outcomes, thus indicating an insufficiency in accurately delineating the inherent properties of water through this methodology.
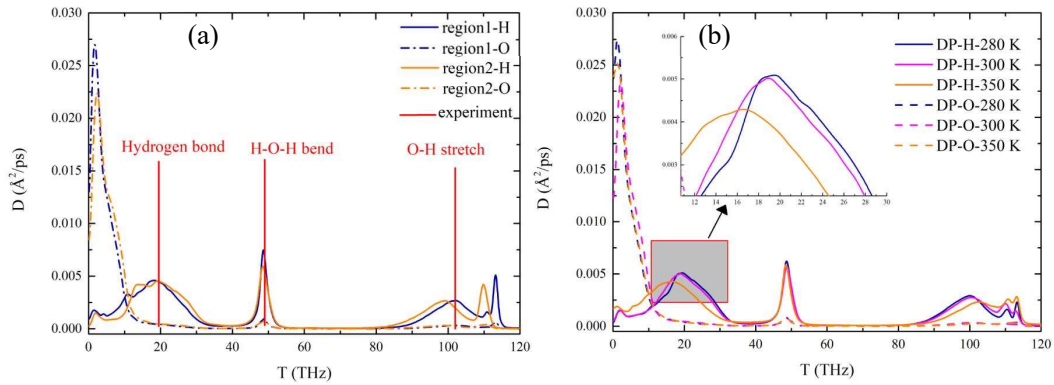
Figure 3. (a) The comparison of power spectra of water calculated by DP and experiment[46] at 280

K. (b) The power spectra of water at three different temperatures calculated by DP.

The effect of temperature on the vibrational power spectrum of water was also investigated. It was found that in Fig. 3(b), the low-frequency region of the vibrational power spectrum undergoes a redshift as temperature ascends. This spectral shift is predominantly rooted in the thermal-induced restructuring of the hydrogen bonding network, a dynamic interplay that subsequently modulates the intermolecular interactions within the network. At elevated temperatures, the stability of the hydrogen bonding network is compromised, leading to a diminution in the strength of hydrogen bonding interactions. This thermally-induced weakening facilitates the disruption of the hydrogen bonding network, thus impacting the vibration frequency. In Fig. 3(b), the temperature has a significant effect on the vibrational absorption peaks of the hydrogen bonding network of water. However, it has a limited effect on the absorption peaks of the bending and stretching vibrations of water. In conclusion, the presence of π-bonds in graphene affects the motion of water molecules within the ionic solution, which in turn affects the properties.

The density profile is a key parameter that assess the influence of the cation-π in the system. In this segment, the density of the system under 280 K,300 K and 350 K is investigated utilizing the LAMMPS with DP and UFF potentials. As illustrated in Fig. 4, the results reveal that the density of graphene surface as calculated using the DP is approximately triple that determined through the UFF. This pronounced disparity underscores the superior strength of the interaction forces exerted on graphene when employing the DP model.

Furthermore, a phenomenon was observed with respect to the thickness of the high-density layer near the graphene surface. It was found that the thickness of the liquid film increased from 2 to 3 nm at elevated temperatures. For the DP, a separation of molecular clusters occurred at 350 K. This phenomenon can be attributed to the increase in the kinetic energy of the system ions, which enhances the intermolecular motion.

Meanwhile, the fundamental divergence in interaction forces, as encapsulated by the DP and UFF models, stands as the cardinal driver behind the enrichment effect observed on the graphene surface. This effect, in turn, cascades into discernible alterations in surface density distribution and intrinsic wettability characteristics[48]. These deviations from the predictions rendered by the UFF method underscore the necessity for adopting advanced computational models, such as the DP framework, to accurately decipher and represent the complex interplay between hydrated cation and graphene surfaces. These insights differ from the prevailing view and highlight the key role that deep learning plays in elucidating the properties of ionic solutions on graphene surfaces.
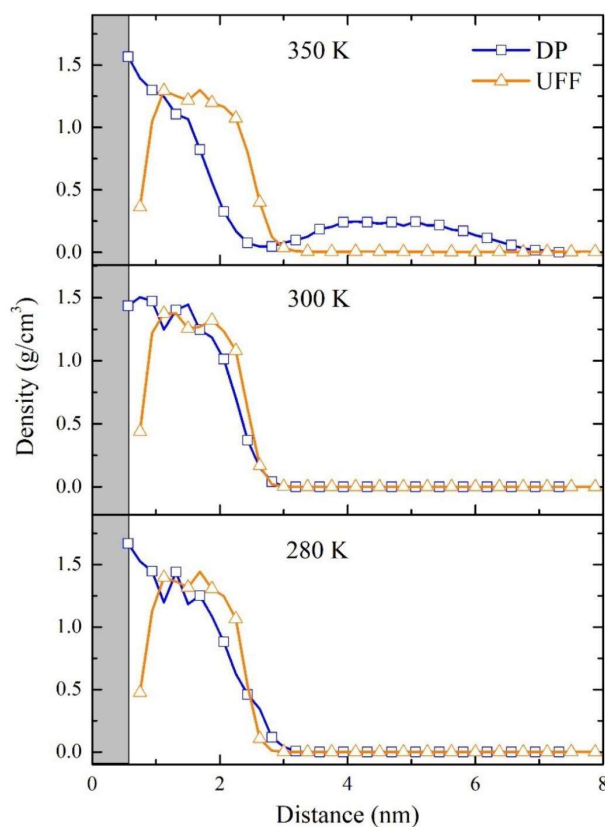
Figure 4. Density profile of the solution under different temperature (the grey areas represent single-layer graphene wall)

The MSD is a covariate that quantifies the diffusion capacity, facilitating a nuanced exploration of the impact exerted by hydrated cation-π interactions on diffusive processes. MSD distribution in the z-direction (orthogonal to the graphene plane) for the ion solution, meticulously computed at 280 K, was calculated quantitatively in Fig. 5. A substantial disparity exists between the MSD values derived from the DP and UFF potential. The UFF potential demonstrates a swifter attainment of equilibrium, accompanied by a more pronounced fluctuation in MSD values as temperatures rise. This divergence suggests that the DP model engenders stronger interatomic interaction forces. These findings unquestionably demonstrate the existence of unique interaction forces between hydrated cation and graphene (cation-π interaction), which are not

accounted for by the universal force field.

The combination of ions and water molecules in solution systems results in the formation of hydrated cation, which exert an influence on the properties of the solution. However, the amount of bound water around Cs^+ is not well known. We have embarked upon an analysis involving radial distribution function (RDF) and coordination number calculations. As illustrated in Fig. S2, the relationship between Cs^+ and water molecules is described by RDF curves using the DP and UFF. Both RDF peak in the vicinity of 0.33 nm. the DP shows that the coordination number in the first solvation shell agrees with that of the UFF potential[21].
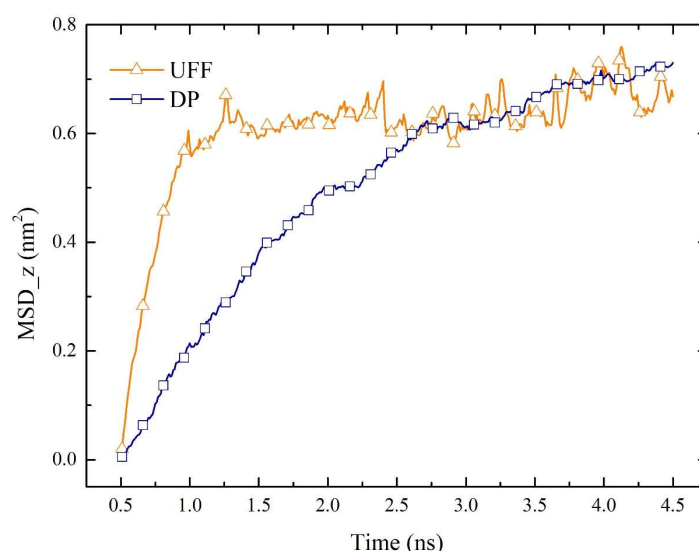

Figure 5. The comparisons of mean square displacement along z-direction by using UFF and DP at 280 K.

To understand the adsorption mechanism of hydrated Cs^+ on graphene surfaces, it is analyzed that the molecular orbitals and electronic structures. This approach allowed us to confidently identify the key factors contributing to the adsorption mechanism. The electronic structure analysis was based on the total density of states (TDOS) and the project density of states (PDOS), which provided an energy level distribution of

molecular orbitals and allowed for analysis of the contribution of each orbital. Fig. 6(a) displays the energy band densities of Cs^+ and hydrated Cs^+, revealing a shift that causes electrons to migrate within their empty orbitals. A comparison of Fig. 6(b) reveals that the presence of water molecules disrupts the electron orbital distribution of the Cs^+, thereby corroborating the existence of electron migration within the hydrated cation.

Fig. 6(c) illustrates that graphene and water molecules are the dominant contributors to the TDOS in the case of graphene and hydronium ions. This also elucidates the underlying cause and nature of the strong cation-π interaction force between hydrated cations and graphene. In Fig. 3(a), the explanation that the change in the vibrational frequency of the hydrogen-oxygen bond is due to the migration of electrons in the orbitals of graphene and water molecules is reasonable.

In this discussion, we have conclusively elucidated that the interaction force between hydrated cations and the graphene surface is fundamentally due to the intricate interplay of electron migration. Specifically, this phenomenon involves electron transfer between graphene's intrinsic π-electron cloud and the molecular orbitals of the hydrated ions. This electrostatic force arises from the redistribution of charge density. This results in a strong electrostatic force that plays a key role in consolidating the affinity of hydrated cations for graphene. In essence, our findings not only elucidate the microscopic mechanism of the interaction between hydrated cations and graphene, but also contribute to a broader understanding of the interaction between ions and π-electrons. This knowledge provides a theoretical foundation for subsequent ion adsorption and ion filtration.
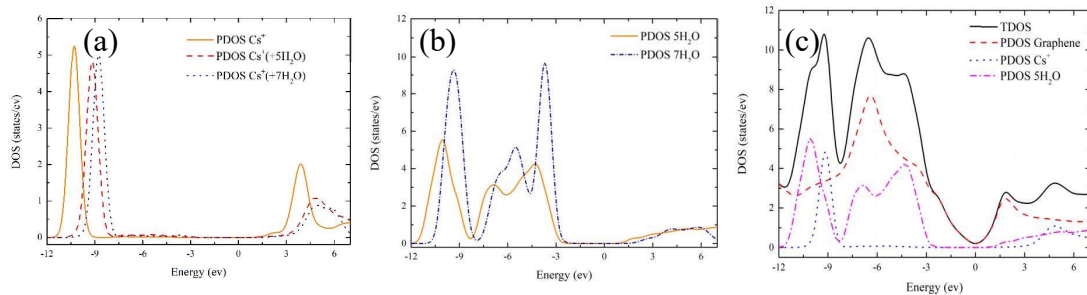
Figure 6. (a) The project density of states of Cs^+ and Cs^+ in hydrated cation; (b) The density of states of water in hydrated cations; (c) The total and project density of states of system

Conclusion

Here, machine learning techniques were employed to train and validate the hydrated Cs^+-π interaction deep potential and predict solution properties. The accuracy of DP is much higher than UFF by comparisons.

By using molecular dynamics simulation, it is found that the water vibration power spectrum calculated by DP matches well with the experimental results. And the presence of π-bonds dampens the vibration frequency at 102 THz. This is mainly due to electron transfer affecting the strength of the hydroxyl bonds.

Furthermore, the distribution of density on the surface of graphene was calculated. It was found that the density calculated by DP was three times higher than that of UFF. The MSD along the z-direction, calculated by DP, was found to be significantly smaller than that calculated by UFF. This can be attributed to the strong interaction forces between graphene and hydrated ions, which cannot be described by the UFF. The hydrated Cs^+-π interaction force is attributed to the migration of electrons in the graphene π-bonds and the molecular orbitals of the hydrated Cs^+, resulting in a strong electrostatic interaction.

These findings not only deepen the understanding of the intricate interactions between hydrated ions and the graphene surface, but also have important implications for the adsorption and removal of radioactive ions on graphene substrates. A theoretical framework is established for the development of graphene-based materials with enhanced ion adsorption and filtration capabilities.

Reference

[1] Zhang X., Liu Y. Nanomaterials for radioactive wastewater decontamination[J]. Environmental Science: Nano,2020;7: 1008-1040.

[2] Fuks L., Herdzik-Koniecko I., Kiegiel K., et al. Management of Radioactive Waste Containing Graphite: Overview of Methods[J]. Energies,2020;13: 4638.

[3] Zhang X., Gu P., Liu Y. Decontamination of radioactive wastewater: State of the art and challenges forward[J]. Chemosphere,2019;215: 543-553.

[4] Inose S., Nanri Y., Saito R., et al. CHARACTERISATION OF RADIOACTIVE CAESIUM IN SEDIMENTS AT THE NOGAWA RIVER, JAPAN[J]. Radiation Protection Dosimetry,2022;198: 909-913.

[5] Teow Y.H., Mohammad A.W. New generation nanomaterials for water desalination: A review[J]. Desalination,2019;451: 2-17.

[6] Rana D., Matsuura T., Kassim M.A., et al. Radioactive decontamination of water by membrane processes — A review[J]. Desalination,2013;321: 77-92.

[7] Li G., Qi X., Yang N., et al. Novel iron-supported ZSM-5 molecular sieve remove arsenic from wastewater by heterogeneous nucleation with pH limit breaking[J]. Chemosphere,2022;301: 134676.

[8] Vereshchagina T.A., Vereshchagin S.N., Shishkina N.N., et al. Microsphere zeolite materials derived from coal fly ash cenospheres as precursors to mineral-like aluminosilicate hosts for 135,137Cs and 90Sr[J]. Journal of Nuclear Materials,2013;437: 11-18.

[9] Park Y., Lee Y.-C., Shin W.S., et al. Removal of cobalt, strontium and cesium from

radioactive laundry wastewater by ammonium molybdophosphate–polyacrylonitrile (AMP–PAN)[J]. Chemical Engineering Journal,2010;162: 685-695.

[10]   Yin L., Kong X., Shao X., et al. Synthesis of DtBuCH18C6-coated magnetic metal–organic framework Fe3O4@UiO-66-NH2 for strontium adsorption[J]. Journal of Environmental Chemical Engineering,2019;7: 103073.

[11]   Zhou K., Zhu Y., Yang X., et al. Preparation of graphene–TiO2 composites with enhanced photocatalytic activity[J]. New Journal of Chemistry,2011;35: 353-359.

[12]   Zeng J., Zhang Y., Chen Y., et al. Molecular dynamics simulation of the adsorption properties of graphene oxide/graphene composite for alkali metal ions[J]. Journal of Molecular Graphics and Modelling,2022;114: 108184.

[13]   Li S., Zhang X., Su J. Surface modification promotes the desalination performance in asymmetric graphene channels[J]. Journal of Molecular Liquids,2023;386: 122448.

[14]   Zhao G., Zhu H. Cation–π Interactions in Graphene-Containing Systems for Water Treatment and Beyond[J]. Advanced materials,2020;32: 1905756.

[15]   Qin Y., Zhao J., Liu Z., et al. Study on effect of different surface roughness on nanofluid flow in nanochannel by using molecular dynamics simulation[J]. Journal of Molecular Liquids,2022;346: 117148.

[16]   Thompson A.P., Aktulga H.M., Berger R., et al. LAMMPS - a flexible simulation tool for particle-based materials modeling at the atomic, meso, and continuum scales[J]. Computer Physics Communications,2022;271: 108171.

[17]   Mu L., Shi G., Fang H. Hydrated cation–π interactions of π-electrons with hydrated Mg2+ and Ca2+ cations[J]. The Journal of Chemical Physics,2024;160.

[18] Mu L., Yang Y., Liu J., et al. Hydrated cation–π interactions of π-electrons with hydrated Li+, Na+, and K+ cations[J]. Physical Chemistry Chemical Physics,2021;23: 14662-14670.

[19] Shi G., Liu J., Wang C., et al. Ion Enrichment on the Hydrophobic Carbon-based Surface in Aqueous Salt Solutions due to Cation-π Interactions[J]. Scientific Reports,2013;3: 3436.

[20] Shi G., Ding Y., Fang H. Unexpectedly strong anion–π interactions on the graphene flakes[J]. Journal of Computational Chemistry,2012;33: 1328-1337.

[21] Chen L., Shi G., Shen J., et al. Ion sieving in graphene oxide membranes via cationic control of interlayer spacing[J]. Nature,2017;550: 380-383.

[22] Williams C.D., Dix J., Troisi A., et al. Effective Polarization in Pairwise Potentials at the Graphene–Electrolyte Interface[J]. The Journal of Physical Chemistry Letters,2017;8: 703-708.

[23] Aydin F., Moradzadeh A., Bilodeau C.L., et al. Ion Solvation and Transport in Narrow Carbon Nanotubes: Effects of Polarizability, Cation−π Interaction, and Confinement[J]. Journal of Chemical Theory and Computation,2021;17: 1596-1605.

[24] Wan X., Ma D., Pan D., et al. Optimizing thermal transport in graphene nanoribbon based on phonon resonance hybridization[J]. Materials Today Physics,2021;20: 100445.

[25] Gao W., Shen L., Sun S., et al. Forecasting solar still performance from conventional weather data variation by machine learning method[J]. Chinese Physics B,2023;32: 048801.

[26] Kohn W., Sham L.J. Self-Consistent Equations Including Exchange and Correlation

Effects[J]. Physical Review,1965;140: A1133-A1138.

[27] Wen T., Zhang L., Wang H., et al. Deep potentials for materials science[J]. Materials Futures,2022;1: 022601.

[28] Tisi D., Zhang L., Bertossa R., et al. Heat transport in liquid water from first-principles and deep neural network simulations[J]. Physical Review B,2021;104: 224202.

[29] Zeng J., Zhang D., Lu D., et al. DeePMD-kit v2: A software package for deep potential models[J]. The Journal of Chemical Physics,2023;159.

[30] He R., Wu H., Zhang L., et al. Structural phase transitions in SrTiO3 from deep potential molecular dynamics[J]. Physical Review B,2022;105: 064104.

[31] Bartók A.P., Payne M.C., Kondor R., et al. Gaussian Approximation Potentials: The Accuracy of Quantum Mechanics, without the Electrons[J]. Physical Review Letters,2010;104: 136403.

[32] Shapeev A.V. Moment Tensor Potentials: A Class of Systematically Improvable Interatomic Potentials[J]. Multiscale Modeling & Simulation,2016;14: 1153-1173.

[33] Chen C., Deng Z., Tran R., et al. Accurate force field for molybdenum by machine learning large materials data[J]. Physical Review Materials,2017;1: 043603.

[34] Sauceda H.E., Chmiela S., Poltavsky I., et al. Molecular force fields with gradient-domain machine learning: Construction and application to dynamics of small molecules with coupled cluster forces[J]. The Journal of Chemical Physics,2019;150.

[35] Zhang L., Lin D.-Y., Wang H., et al. Active learning of uniformly accurate interatomic potentials for materials simulation[J]. Physical Review Materials,2019;3: 023804.

[36] Wu J., Zhou E., Huang A., et al. Deep-potential enabled multiscale simulation of gallium

nitride devices on boron arsenide cooling substrates[J]. Nature Communications,2024;15: 2540.

[37] Shi Y., He R., Zhang B., et al. Revisiting the phase diagram and piezoelectricity of lead zirconate titanate from first principles[J]. Physical Review B,2024;109: 174104.

[38] Zhang L., Wang H., Car R., et al. Phase Diagram of a Deep Potential Water Model[J]. Physical Review Letters,2021;126: 236001.

[39] Zhao W., Qiu H., Guo W. A Deep Neural Network Potential for Water Confined in Graphene Nanocapillaries[J]. The Journal of Physical Chemistry C,2022;126: 10546-10553.

[40] Zhang Y., Wang H., Chen W., et al. DP-GEN: A concurrent learning platform for the generation of reliable deep learning based potential energy models[J]. Computer Physics Communications,2020;253: 107206.

[41] Li K., Persaud D., Choudhary K., et al. Exploiting redundancy in large materials datasets for efficient machine learning with less data[J]. Nature Communications,2023;14: 7283.

[42] Asthagiri D.N., Beck T.L. MD Simulation of Water Using a Rigid Body Description Requires a Small Time Step to Ensure Equipartition[J]. Journal of Chemical Theory and Computation,2024;20: 368-374.

[43] Rappe A.K., Casewit C.J., Colwell K.S., et al. UFF, a full periodic table force field for molecular mechanics and molecular dynamics simulations[J]. Journal of the American Chemical Society,1992;114: 10024-10035.

[44] Stukowski A. Visualization and analysis of atomistic simulation data with OVITO–the Open Visualization Tool[J]. Modelling and Simulation in Materials Science and

Engineering,2010;18: 015012.

[45] Gittus O.R., Bresme F. Thermophysical properties of water using reactive force fields[J]. The Journal of Chemical Physics,2021;155.

[46] Heyden M., Sun J., Funkner S., et al. Dissecting the THz spectrum of liquid water from first principles via correlations in time and space[J]. Proceedings of the National Academy of Sciences,2010;107: 12068-12073.

[47] Bertie J.E., Lan Z. Infrared Intensities of Liquids XX: The Intensity of the OH Stretching Band of Liquid Water Revisited, and the Best Current Values of the Optical Constants of H2O(l) at 25°C between 15,000 and 1 cm−1[J]. Applied Spectroscopy,1996;50: 1047-1057.

[48] Zhang J., Jia K., Huang Y., et al. Intrinsic Wettability in Pristine Graphene[J]. Advanced materials,2022;34: 2103620.

Conflicts of interest

There are no conflicts of interest to declare

Authorship contribution statement: Yangjun Qin: Investigation, Writing - original draft, Data curation, Formal analysis. Xiao Wan: Investigation, Writing - original draft, Data curation. Liuhua Mu: Investigation, Writing - original draft, Software. Zhicheng Zong: Investigation, Writing - original draft, Software. T ianhao Li: Investigation, Writing - original draft, Software. Nuo Yang: Project administration, Conceptualization, Writing - review & editing.

Acknowledgements

Data availability

The data supporting this study's findings are available from the corresponding author upon reasonable request.